Pergamon

Atmospheric Environment Vol. 29, No. 16, pp. 2099–2111, 1995

1352-2310/95 $9.50 + 0.00

1352-2310(94)00288-6

SIMULATION OF ELEVATED LONG-RANGE PLUME TRANSPORT USING A MESOSCALE METEOROLOGICAL MODEL

ZAFER BOYBEYI* and SETHU RAMAN

Department of Marine, Earth and Atmospheric Sciences, North Carolina State University, Raleigh, NC 27695-8208, U.S.A.

(*First received* 16 *February* 1993 *and in final form* 13 *July* 1994)

Abstract—A three-dimensional mesoscale meteorological model was used to construct a modeling system in order to investigate atmospheric dispersion in mesoscale flow fields. The mesoscale model was first coupled to a three-dimensional Monte Carlo (Lagrangian particle) dispersion model, and then an Eulerian dispersion model was embedded into the mesoscale model. Both the Eulerian model and the Monte Carlo model are based on the wind and turbulence fields simulated by the mesoscale model. The modeling system was then applied to the Tennessee Plume Study field experiments on 23 August 1978. The field experiments were basically designed to provide information on the dynamics of plume transport over long distances, and primarily targeted the plume from the Cumberland steam plant. Wind and turbulence fields were first simulated by the mesoscale model. The transport and diffusion of pollutants from the Cumberland steam plant were then simulated by the dispersion models, using these wind and turbulence fields. The results demonstrated that the modeling system generally performed satisfactorily, reproducing the trajectory and spread of the Cumberland plume.

Key word index: Mesoscale modeling, air pollution, Eulerian dispersion, Lagrangian dispersion, Monte Carlo technique, coupled model, long-range transport, Tennessee Plume Study.

1. INTRODUCTION

Over the past decade, there has been growing concern about estimating the long-range transport of pollutants (e.g., Bass, 1980; McNider *et al.*, 1988). This concern has been motivated by relatively new environmental problems such as acid rain, the Chernobyl nuclear disaster, and recently the smoke plumes from the Kuwaiti oil well fires. These problems and their subsequent consequences are international.

In the numerical simulation of long-range transport of pollutants, it is a major problem to determine the correct trajectory of pollutants. Incorrect representation of a meteorological field in dispersion models may result in the transport of pollutants several kilometers away from the actual point (Pack *et al.*, 1978). Therefore, detailed and precise meteorological information is of pivotal importance for modeling the long-range transport of pollutants. This level of information can only be provided by either interpolated meteorological observations or numerical meteorological models. Until recently, the general approach was to use interpolated meteorological observations. In general, the observations are too coarse in both time and space to depict accurately local circulations. One approach to overcome the limitations of the existing meteorological observations is to use the information predicted by meteorological models.

In this study, a modeling system was developed based on coupling a mesoscale meteorological model with a Monte Carlo (Lagrangian particle) dispersion model, plus embedding an Eulerian dispersion model into the mesoscale meteorological model. The modeling system was then applied to the Tennessee Plume Study field experiments on 23 August 1978. The experiments were basically designed to provide information on the dynamics of plume transport over long distances, and primarily targeted the plume from the Cumberland steam plant. The mesoscale flow field was first simulated by the mesoscale meteorological model. The associated plume transport and diffusion from the Cumberland steam plant were then evaluated using both the dispersion models.

2. DESCRIPTION OF THE MODELING SYSTEM

A systematic representation of the modeling system is shown in Fig. 1. A brief description of each model used in the system is given below.

* Present affiliation: SAIC, 1710 Goodridge Drive, McLean, VA 22102, U.S.A.

AE 29-16-0

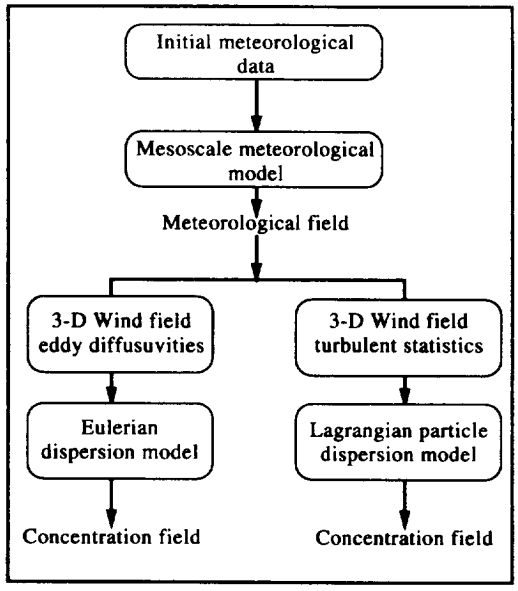

Fig. 1. Systematic representation of the modeling system.

2.1. *Mesoscale meteorological model*

The mesoscale meteorological model used in this study is described in detail by Huang and Raman (1990, 1992), and similar to that used in Boybeyi and Raman (1992a, b). Thus, only a brief description of the model is given here. The model is hydrostatic and anelastic in a terrain-following coordinate system. The governing equations for the mean variables are

$$\frac{\partial u}{\partial t} = -u\frac{\partial u}{\partial x} - v\frac{\partial u}{\partial y} - \tilde{w}\frac{\partial u}{\partial \sigma} + fv - \theta_v\frac{\partial \pi}{\partial x} - g(1-\sigma)\frac{\partial \hat{E}}{\partial x} + \frac{\partial}{\partial x}\left(K_H\frac{\partial u}{\partial x}\right) + \frac{\partial}{\partial y}\left(K_H\frac{\partial u}{\partial y}\right) + \frac{1}{H-\hat{E}}\frac{\partial}{\partial \sigma}\overline{(-u'w')}, \quad (1)$$

$$\frac{\partial v}{\partial t} = -u\frac{\partial v}{\partial x} - v\frac{\partial v}{\partial y} - \tilde{w}\frac{\partial v}{\partial \sigma} - fu - \theta_v\frac{\partial \pi}{\partial y} - g(1-\sigma)\frac{\partial \hat{E}}{\partial y} + \frac{\partial}{\partial x}\left(K_H\frac{\partial v}{\partial x}\right) + \frac{\partial}{\partial y}\left(K_H\frac{\partial v}{\partial y}\right) + \frac{1}{H-\hat{E}}\frac{\partial}{\partial \sigma}\overline{(-v'w')}, \quad (2)$$

$$\frac{\partial \theta}{\partial t} = -u\frac{\partial \theta}{\partial x} - v\frac{\partial \theta}{\partial y} - \tilde{w}\frac{\partial \theta}{\partial \sigma} + \frac{\partial}{\partial x}\left(K_H\frac{\partial \theta}{\partial x}\right) + \frac{\partial}{\partial y}\left(K_H\frac{\partial \theta}{\partial y}\right) + \frac{1}{H-\hat{E}}\frac{\partial}{\partial \sigma}\overline{(-w'\theta')} - \frac{L_c}{\pi}\left(\delta\frac{dq_s}{dt}\right) + Q_{CL} - Q_{EV} + Q_{RAD}, \quad (3)$$

$$\frac{\partial q}{\partial t} = -u\frac{\partial q}{\partial x} - v\frac{\partial q}{\partial y} - \tilde{w}\frac{\partial q}{\partial \sigma} + \frac{\partial}{\partial x}\left(K_H\frac{\partial q}{\partial x}\right) + \frac{\partial}{\partial y}\left(K_H\frac{\partial q}{\partial y}\right) + \frac{1}{H-\hat{E}}\frac{\partial}{\partial \sigma}\overline{(-w'q')} + \delta\frac{dq_s}{dt} + M_{CL} + M_{EV}, \quad (4)$$

$$\frac{\partial q_c}{\partial t} = -u\frac{\partial q_c}{\partial x} - v\frac{\partial q_c}{\partial y} - \tilde{w}\frac{\partial q_c}{\partial \sigma} + \frac{\partial}{\partial x}\left(K_H\frac{\partial q_c}{\partial x}\right) + \frac{\partial}{\partial y}\left(K_H\frac{\partial q_c}{\partial y}\right) + \frac{1}{H-\hat{E}}\frac{\partial}{\partial \sigma}\overline{(-w'q_c')} - \delta\frac{dq_s}{dt} - M_{AC} - M_{RV}, \quad (5)$$

$$\frac{\partial q_r}{\partial t} = -u\frac{\partial q_r}{\partial x} - v\frac{\partial q_r}{\partial y} - \tilde{w}\frac{\partial q_r}{\partial \sigma} + \frac{\partial}{\partial x}\left(K_H\frac{\partial q_r}{\partial x}\right) + \frac{\partial}{\partial y}\left(K_H\frac{\partial q_r}{\partial y}\right) + \frac{1}{H-\hat{E}}\frac{\partial}{\partial \sigma}\overline{(-w'q_r')} + M_{VT} + M_{AC} + M_{RV} - M_{EV}, \quad (6)$$

$$\frac{\partial \rho u(H-\hat{E})}{\partial x} + \frac{\partial \rho v(H-\hat{E})}{\partial y} + \frac{\partial \rho \tilde{w}(H-\hat{E})}{\partial \sigma} = 0, \quad (7)$$

$$\frac{\partial \pi}{\partial \sigma} = -\frac{g(H-\hat{E})}{\theta_v}, \quad (8)$$

where the terrain-following coordinate is defined as

$$\sigma = \frac{z-\hat{E}}{H-\hat{E}}, \quad (9)$$

using the height of the model domain H, and the terrain height, $\hat{E}$. Equations (1) and (2) are the horizontal momentum (u and v) equations for eastwest and northsouth directions, respectively. Equation (3) is the thermodynamic equation for the potential temperature, θ. Equations (4), (5) and (6) are the conservation equations for water vapor, q, cloud water, q_c and rain water, q_r, respectively. Equation (7) is the anelastic equation for fluid continuity.

To close the governing equations, unknown turbulent flux terms are required to be specified by mean fields. The similarity relationships given by Businger *et al.* (1971) are used for the surface layer in the model. Above the surface layer, a turbulence closure scheme based on two prognostic equations, one for the turbulent kinetic energy, E, and the other for turbulent energy dissipation, ε, is incorporated with the level 2.5 scheme of Mellor and Yamada (1982) to determine vertical eddy diffusivities. After considerable algebraic reduction, the final forms of vertical eddy diffusivities for momentum, heat, and moisture in the level 2.5 formulation are expressed as

$$K_M = c_1 l(2E)^{1/2} S_M, \quad (10)$$

$$K_\theta = K_q = c_1 l(2E)^{1/2} S_H, \quad (11)$$

where S_M and S_H are the non-dimensional functions reported by Mellor and Yamada (1982), l the eddy mixing length parameterized for different stability conditions in terms of the known variables, E the turbulent kinetic energy, and c_1 a closure constant. The horizontal eddy diffusivity, K_H, in the model is assumed in the form discussed by Pielke (1984);

$$K_H = \alpha_H \Delta x \Delta y \left\{ \left(\frac{\partial v}{\partial x} + \frac{\partial u}{\partial y} \right)^2 + \frac{1}{2} \left[\left(\frac{\partial u}{\partial x} \right)^2 + \left(\frac{\partial v}{\partial y} \right)^2 \right] \right\}^{1/2}, \quad (12)$$

where α_H is a constant of order one.

To account for advection effects, a modified version of the Warming–Kutler–Lomax advection scheme (Warming *et al.*, 1973) is used in the horizontal and the quadratic upstream interpolation in the vertical, while all vertical diffusion terms are computed by a time-implicit scheme. At the lower boundary, a no-slip condition is imposed for the wind. The water surface temperature is fixed, while the land surface temperature is computed by numerically integrating the force-restore equation (Bhumralkar, 1975; Deardorff, 1978). Relative humidity for the land surface remains unchanged, but the air in contact with the water surface is assumed to be saturated. The hydrostatic equation is used to obtain the surface pressure with the known upper level pressure. At the upper boundary, a radiation boundary condition (Klemp and Durran, 1983) is used to determine the upper perturbation pressure. Orlanski's radiation condition (Orlanski, 1976) with forward-upstream scheme (Miller and Thorpe, 1981) is applied to the prognostic variables at lateral boundary grids.

2.2. *Eulerian dispersion model*

Basically, all Eulerian dispersion models solve the advection-diffusion equation in a fixed frame reference. There are several aspects in which one model can differ from another, such as the specification of initial and boundary conditions, numerical techniques, parameterization of eddy diffusivities, and simplifying assumptions. The following form of the advection–diffusion equation for the change of pollutant concentrations, C, with time t in the σ terrain following coordinate system is embedded into the mesoscale meteorological model;

$$\frac{\partial C}{\partial t} = -u\frac{\partial C}{\partial x} - v\frac{\partial C}{\partial y} - \dot{w}\frac{\partial C}{\partial \sigma} + \frac{\partial}{\partial x}\left(K_H \frac{\partial C}{\partial x} \right) + \frac{\partial}{\partial y}\left(K_H \frac{\partial C}{\partial y} \right) + \frac{1}{H - \hat{E}} \frac{\partial}{\partial \sigma} \overline{(-w'C')} + S_C, \quad (13)$$

where S_C is the source term. Vertical turbulent transport of concentration is carried out using the same turbulent closure scheme prescribed in the mesoscale model, while the horizontal eddy diffusivity coefficient, K_H, is computed using the same nonlinear smoothing presented in equation (12).

The vertical boundary conditions assume complete reflection of concentration at the ground surface, while the prediction equation is used at the model top. The domain lateral size is specified to contain most of the plume. Nevertheless, the choice of boundary conditions on the lateral boundary is important in order to avoid reflection or absorption from these boundaries. The same lateral boundary condition prescribed in the mesoscale model is applied to the concentration field. The same numerical techniques used in the mesoscale meteorological model are also used for the numerical solution of equation (13).

2.3. *Monte Carlo dispersion model*

The Monte Carlo dispersion model used in this study was originally developed by Zannetti (1984, 1986) and coupled to the mesoscale meteorological model by Boybeyi *et al.* (1994). The model simulates the dispersion of dynamically passive pollutants in the atmosphere by means of a large ensemble of Lagrangian particles moving with pseudo-velocities. The Monte Carlo model assigns a horizontal wind aligned local coordinate system for each particle at each time step based on the horizontal mean wind direction at the particle location. In this local coordinate system, the x-axis is chosen to coincide with the mean wind direction. The choice of x-axis in the mean wind direction simplifies the treatment of the cross-correlation terms, since in this local reference system it can be assumed that only the cross correlation $\overline{u'w'}$ is non-zero. Particle positions are then computed from the following relations:

$$\begin{aligned} x(t + \Delta t) &= x(t) + [\bar{u}(t) + u'(t)]\Delta t, \\ y(t + \Delta t) &= y(t) + [v'(t)]\Delta t, \\ z(t + \Delta t) &= z(t) + [\bar{w}(t) + w'(t)]\Delta t, \end{aligned} \quad (14)$$

where $\bar{u}$ and $\bar{w}$ represent the horizontal mean and vertical velocity components obtained from the mesoscale model resolved eastwest, northsouth, and vertical velocity components. Since the grid-scale meteorological variables are defined only on the mesoscale model grid mesh, a linear interpolation scheme is used to estimate their values at each particle location.

The semi-random turbulent velocity fluctuations are generated by the following Monte Carlo scheme:

$$\begin{aligned} u'(t + \Delta t) &= \phi_1 u'(t) + u''(t + \Delta t), \\ v'(t + \Delta t) &= \phi_2 v'(t) + v''(t + \Delta t), \\ w'(t + \Delta t) &= \phi_3 w'(t) + \phi_4 u'(t + \Delta t) + w''(t + \Delta t), \end{aligned} \quad (15)$$

where u'', v'' and w'' are purely random, independent, and uncorrelated turbulent velocity fluctuations (i.e., "white noise"). These random fluctuations are taken to be Gaussian with zero mean and the following

variances:

$$\sigma_{u'}^2 = \sigma_u^2(1 - \phi_1^2), \qquad \sigma_{v'}^2 = \sigma_v^2(1 - \phi_2^2), \quad (16)$$
$$\sigma_{w'}^2 = \sigma_w^2(1 - \phi_3^2) - \phi_4^2\sigma_{u'}^2 - 2\phi_1\phi_3\phi_4 R_{u'w'}\sigma_{u'}\sigma_{w'},$$

where $\sigma_{u'}$, $\sigma_{v'}$ and $\sigma_{w'}$, are the turbulent velocity standard deviations. The parameters ϕ_1, ϕ_2, ϕ_3, and ϕ_4 in equations (15) and (16) are computed using the following algebraic manipulations:

$$\phi_1 = R_{u'}, \qquad \phi_2 = R_{v'},$$
$$\phi_3 = \frac{R_{w'} - R_{u'}R_{u'w'}^2}{1 - R_{u'}^2 R_{u'w'}^2}, \quad (17)$$
$$\phi_4 = \frac{R_{u'w'}\sigma_{w'}(1 - R_{u'}R_{w'})}{\sigma_{u'}(1 - R_{u'}^2 R_{u'w'}^2)},$$

where autocorrelation coefficients ($R_{u'}$, $R_{v'}$ and $R_{w'}$) and the one required cross-correlation coefficient ($R_{u'w'}$) are described in detail by Zannetti (1990).

The Lagrangian turbulent statistics (turbulent velocity standard deviations; $\sigma_{u'}$, $\sigma_{v'}$, $\sigma_{w'}$, and Lagrangian integral time scales; $T_L^{u'}$, $T_L^{v'}$, $T_L^{w'}$) need to be determined in each of the three component directions. The Monte Carlo model uses the equations for turbulent statistics suggested by Hanna (1982) in which Lagrangian turbulence statistics are related to boundary layer parameters such as friction velocity, u_*, convective velocity, w_*, mixed layer height, h_i, Monin–Obukhov length, L, and surface roughness length, z_0. All these boundary layer parameters (u_*, w_*, h_i, L and z_0) are obtained from the mesoscale meteorological model fields (Boybeyi *et al.*, 1994).

3. METEOROLOGICAL CONDITIONS

This section provides a general review of the meteorological conditions on 23 August 1978. Figure 2 shows the surface weather map at 0700 EST. The location of the Cumberland steam plant is indicated in the figure as CU. A high pressure system was centered over much of the eastern United States. Later during the day, this pressure system drifted slowly southeastward. Frontal activity remained well to the north of the Tennessee Plume Study area. Figure 3 shows satellite pictures for the Tennessee Plume Study area at 0930 and 1330 LST. The location and direction of the Cumberland plume transport are indicated in each picture by an arrow. Sky conditions were clear during the morning. This cloudiness persisted throughout the morning hours and then gradually evolved into an area of mainly stratus and cirrus clouds. It was also observed that the planetary boundary layer was restricted to below 1 km during the morning hours. Later in the afternoon, the boundary layer reached a maximum height of about 1.5 km.

Mesoscale meteorological analysis on 23 August 1978, at 0400, 0700 and 1300 LST are shown in Fig. 4 (after Clark *et al.*, 1980) for the Tennessee Plume Study area. The figure shows an evaluation of meteorological data from the National Weather Service, the Air Weather Service, and the Tennessee Valley Authority. The first chart in the series (Fig. 4a) shows sea level pressure at 1 mbar intervals with solid lines even and dashed lines odd. The second and third charts in the figure show the mean wind flow analysis for the layers 300–750 and 750–1250 m (above mean sea level), respectively. The mean wind information is plotted in

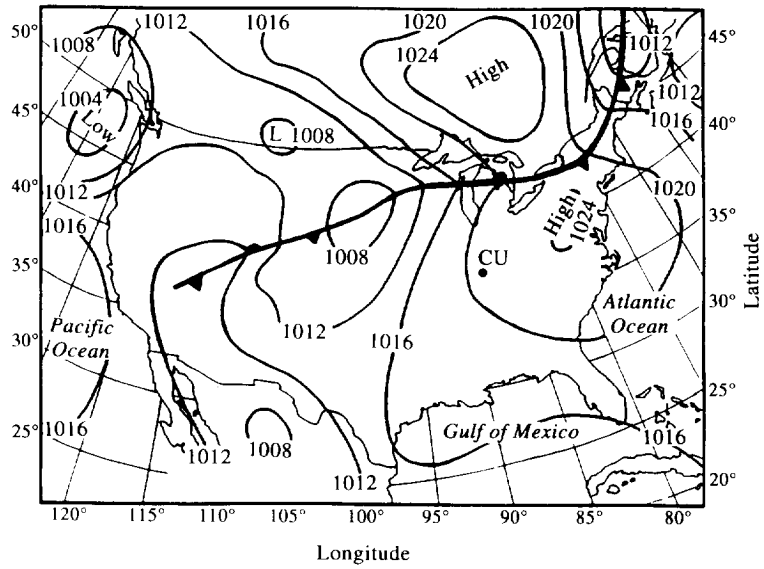

Fig. 2. Surface weather map indicating the analysis for 0700 EST on 23 August 1978. The location of the Cumberland steam plant is indicated in the figure as CU.

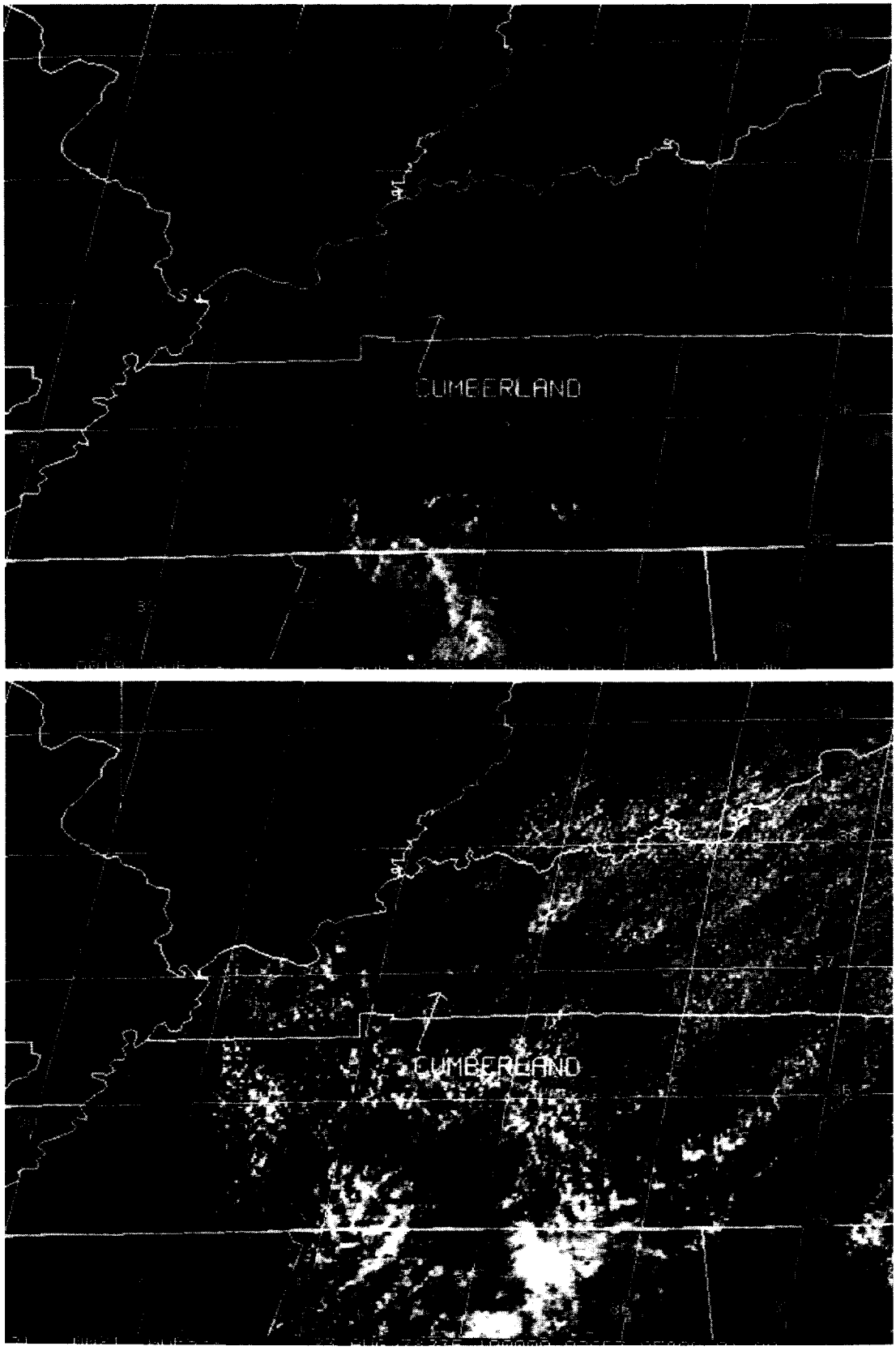

Fig. 3. Satellite pictures of Tennessee Plume Study area showing cloud evolution at 0930 and 1330 LST on 23 August 1978. The direction of the transport of the Cumberland plume is shown in each picture by an arrow.

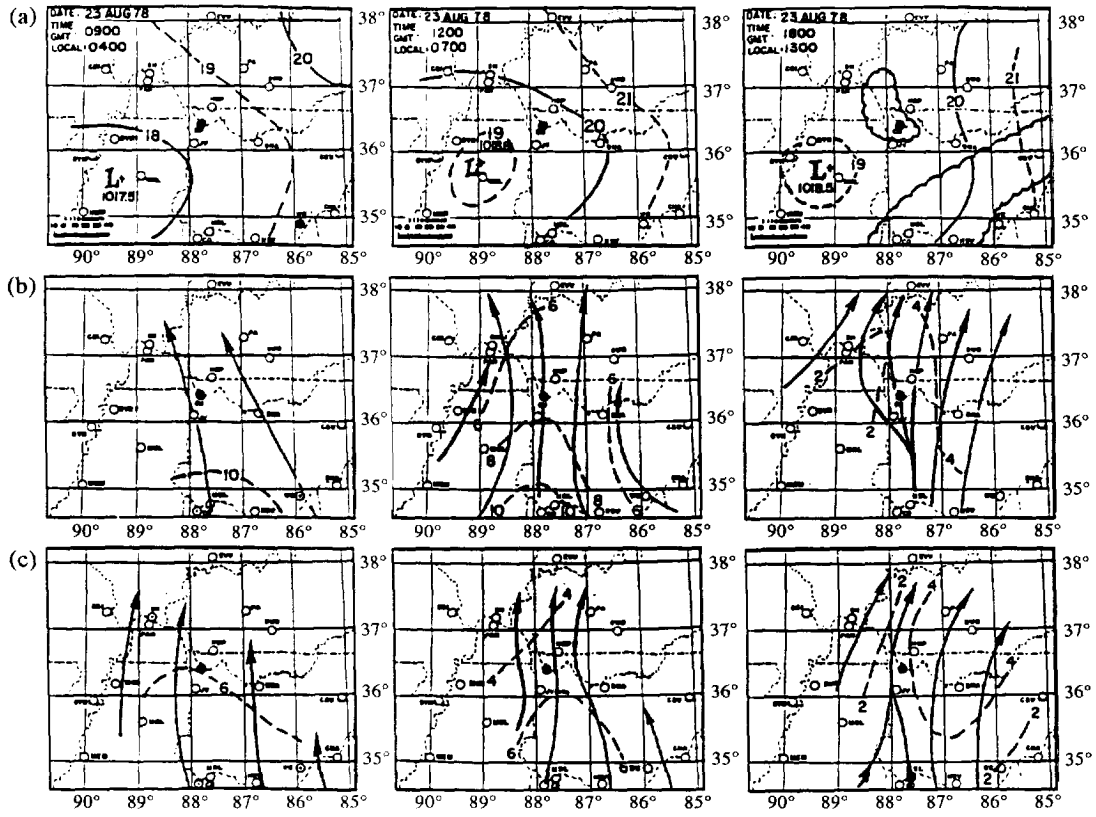

Fig. 4. Mesoscale chart analysis of Tennessee Plume Study area showing (a) surface pressure analysis, (b) mean flow observations for the level 300–750 m, (c) mean flow observations for the level 750–1250 m at 0400, 0700 and 1300 LST on 23 August 1978 (after Clark *et al.*, 1980). The location of the Cumberland plant is indicated with a dark dot.

a simple form. The solid lines with arrows indicate wind direction, while the dashed lines show wind speed in even meters per second. A weak trough over the southwestern portion of the Cumberland gradually developed into a weak low-pressure area during the morning. Later in the afternoon, its center became nearly stationary and then gradually filled during the evening (not shown). Following the mesoscale surface analysis, at the layer 300–750 m, winds were from the southeast with an average speed of about 10 m s^{-1}. Later during the day, the flow changed its direction and became southerly and subsequently southwesterly. Wind speed at this level dropped rapidly from 10 to about 4 m s^{-1} as the turbulent mixing effects became predominant by the afternoon. At the upper level (the layer at 750–1250 m), a shift in the wind direction from south to southwest was also observed. The average wind speed was about 6 m s^{-1} during the early morning. Later in the afternoon the speed decreased to about 4 m s^{-1}.

4. A BRIEF DESCRIPTION OF TENNESSEE PLUME STUDY

The Tennessee Plume Study is fully described in a series of reports (Clark *et al.*, 1980; Gillani *et al.*, 1979a, b). Therefore, only the important features of the study will be outlined here. The United States Environmental Protection Agency (EPA) conducted a major field study at the Tennessee Valley Authority's Cumberland steam plant during August 1978. This study was conducted as part of the EPA Sulfur Transport and Transformation in the Environment Project. The Tennessee Valley Authority, other government agencies, universities, and private organizations participated with EPA in this study, which was known as the Tennessee Plume Study.

The field experiments were basically designed to provide information on the dynamics of plume transport over long distances, and primarily targeted plumes from large power plants, particularly the Cumberland steam plant plume. Around 0700 LST on 23 August 1978, the Cumberland plume was released and sampled at three different downwind distances (80, 110 and 160 km) over a 10 h time period. The corresponding plume ages were about 4, 5.4 and 10 h, respectively. A schematic representation of the trajectory of the Cumberland plume and the sampling locations are shown in Fig. 5 (Gillani *et al.*, 1981). The figure is also representative of the modeling system simulation domain. The measured crosswind concentrations of the Cumberland plume at the downwind

distances of 80, 110 and 160 km are shown in Fig. 6. Aircraft flying time scales (1131–1138, 1224–1231 and 1557–1606 LST) and corresponding travel distances (25, 25 and 32 km) are also indicated in the figure. The measurements at 80 and 110 km were made by the Brookhaven National Laboratory aircraft, and the measurements at 160 km were made by the Environmental Measurements Inc., aircraft. Note that the measured plume widths at 80, 110 and 160 km downwind distances are estimated at about 13, 21 and 27 km and represent three different stages of the plume development: early, intermediate, and mature, respectively.

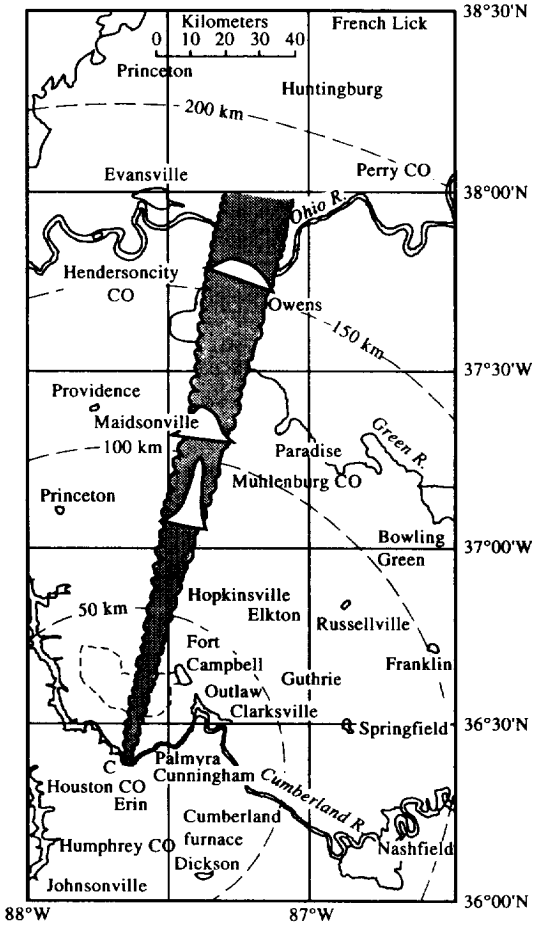

Fig. 5. Map of the Tennessee Plume Study area showing the trajectory of the Cumberland (C) plume and the sampling locations at three different downwind distances (80, 110 and 160 km) on 23 August 1978.

5. MODEL PARAMETERS

The mesoscale meteorological model was initialized using 0455 LST mean sounding data taken at Johnsonville on 23 August 1978. The location of Johnsonville is shown in Fig. 5. The initial vertical profiles of temperature, T, and dew point temperature, T_d, are plotted on a skew-T log-P diagram (Fig. 7). The initial wind information is also plotted on the right-hand side of the figure. These profiles were imposed over the entire model domain at the start of integration. Other important input parameters needed for the mesoscale model are given in Table 1. The mesoscale model

Table 1. The mesoscale meteorological model parameters

Quantity	Value
Day of year	23 August
Mean latitude	36°N
Model start time	0500 LST
Model run time	12 h
Time step	20 s
Grid spacing (Δx, Δy)	5 km
Grid size (x, y, z)	24 × 48 × 15
Roughness length	5 cm
Surface temperature	20°C
Albedo	0.25
Soil thermal diffusivity	0.0018 $cm^2 s^{-1}$
Model top	3 km
Vertical levels	0, 50, 150, 305, 450, 600, 750, 900, 1050, 1250, 1450, 1650, 2050, 2450, 3000 m

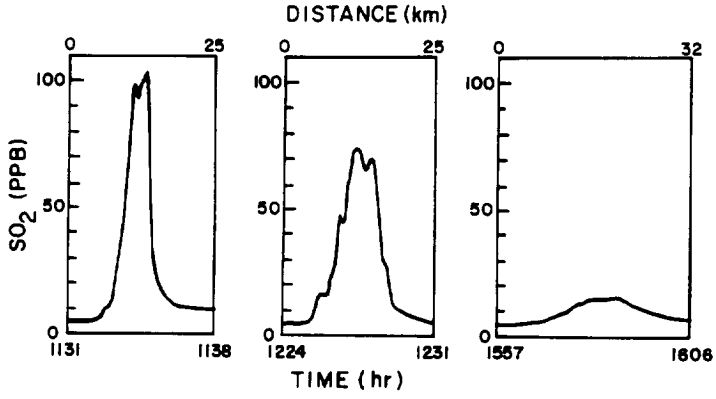

Fig. 6. Crosswind SO_2 concentrations of the Cumberland plume at downwind distances of 80, 110 and 160 km, respectively.

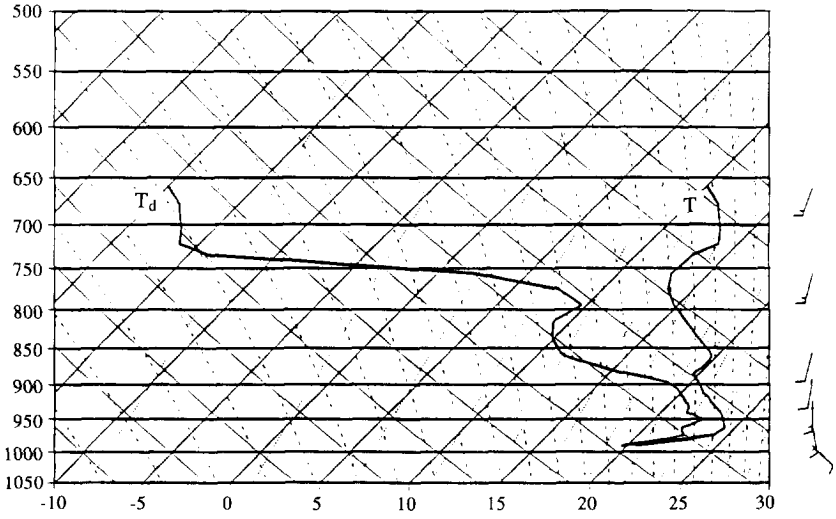

Fig. 7. Mean sounding data taken at Johnsonville at 0455 LST on 23 August 1978 plotted on a skew-T log-P diagram. First solid line on the right-hand side is temperature, T. Second solid line on the left is dew point temperature, T_d. The initial wind information is also plotted on the right-hand side of the figure.

domain contains 15 non-uniform grid levels in the vertical and 24×48 grid points in the horizontal with a uniform grid interval of 5 km. The model is integrated for 12 h after 0500 LST on 23 August 1978. The initial surface temperatures are based on observations. It is assumed that the surface temperature is 20°C. The surface roughness values are assumed to be 5 cm. Both the Eulerian model and the Monte Carlo model simulation begin at 0700 LST and continue for 10 h until 1700 LST with a 20 s time interval. Source height is set at a height of 305 m, with a source strength of about 13 g s^{-1}.

6. DISCUSSION OF RESULTS

Precise and detailed wind information is of pivotal importance in the numerical simulation of long-range plume transport. Figure 8 shows horizontal wind vector fields (u and v) at initial time and after 2 and 8 h of the mesoscale model simulation for a horizontal plane at the source height of 305 m. A comparison of the mesoscale model-simulated wind fields with the mesoscale chart analysis presented in Fig. 4b at equivalent times, shows that direction and speed changes in ambient winds are simulated reasonably well by the mesoscale model. The simulated wind field shows that the southeasterly initial winds become southerly after 2 h of model simulation. Later in the afternoon, the winds become southwesterly and decrease in speed. Changes in the wind direction and magnitude must be due to the turbulence mixing processes.

A comparison between observed and equivalent mesoscale model simulated potential temperature profiles is presented in Fig. 9. The vertical profiles are taken at Johnsonville at 1400 LST. The potential temperature profile is important in determining the characteristics of the turbulence fields. The initial nocturnal surface temperature inversion (Fig. 7) breaks up in the late morning. Later during the day (by 1400 LST), surface heating results in a super adiabatic surface layer near the ground surface and a well-defined mixed layer aloft. The mixed layer attains a depth of about 1.5 km by this hour and is capped aloft by an inversion layer. The vertical potential temperature profile and boundary layer height simulated by the mesoscale model show good agreement with the observed values.

The Eulerian model and the Monte Carlo model, using the wind and turbulence fields from the mesoscale model fields, are then used to simulate transport of the Cumberland plume on 23 August 1978. The Eulerian dispersion model simulated concentration fields after 4, 5.5 and 10 h of plume travel time are shown in Fig. 10 for a horizontal plane at the source height of 305 m. Advective and diffusive growth of the plume shows that the plume changes its direction during the integration in response to the mesoscale model predicted wind fields. The simulated trajectory of the plume is in good agreement with the observed trajectory of the plume. However, the spread of the plume is not handled very well by the Eulerian model. The model produces artificial diffusion, especially near the source. This condition results from concentrations being computed as spatial averages in three-dimensional cells. This is a general problem for all Eulerian dispersion models due to their homogeneous grid cells. The problem results from the limited spatial resolution of such models. In many cases, plumes occupy a volume smaller than the size of one dispersion model grid cell, and do not expand to fill a cell until far downwind. Therefore, the Eulerian model spreads the pollutants

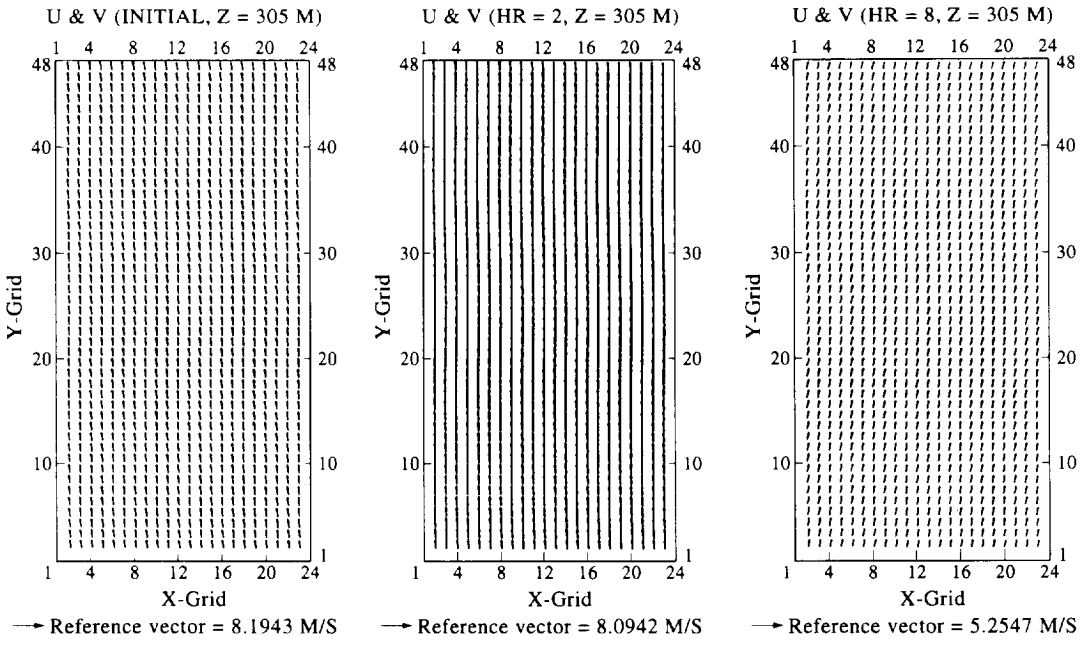

Fig. 8. The mesoscale meteorological model simulated wind vector fields u and v ($m\,s^{-1}$) at the initial stage and after 2 and 8 h of integration for a horizontal plane located at the source height of 305 m.

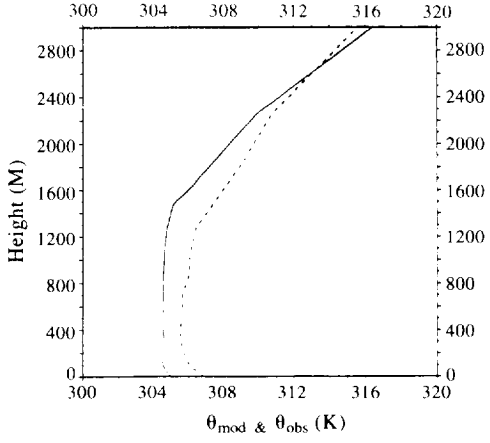

Fig. 9. Observed (dashed line) and the mesoscale meteorological model simulated (solid line) vertical potential temperature profiles at 1400 LST.

over the cell where the source is located, resulting in a substantial initial diffusion near the source. In addition, all numerical advection schemes used in Eulerian models contribute to the aritificial diffusion. This is due the to fact that the advection schemes cannot handle small wavelength features very well and thus additional numerical diffusion is added to the solution.

Figure 11 shows the Eulerian model simulated crosswind concentration values at 80, 110 and 160 km downwind distances after 4, 5.5 and 10 h of plume travel times, respectively. A comparison of these results with those shown in Fig. 6 indicates that the magnitudes of the concentrations are generally underestimated, while the spread of the plume is overestimated due to the reasons discussed above.

Figure 12 shows the Monte Carlo model simulated particle locations projected on a horizontal plane at the source height of 305 m after 4, 5.5 and 10 h of plume travel times. The Monte Carlo model avoids the artificial numerical diffusion associated with the Eulerian method. The treatment of near source dispersion using a point source is handled very well as compared to the Eulerian model simulation. The Monte Carlo model also simulates the spread of the plume in better agreement with the observed plume spread (Fig. 6). However, the use of the Monte Carlo model for long-range transport of pollutants requires release of a large number of particles. When a very large number of particles is released, the computational requirements quickly become unmanageable.

Based on the results presented above, one may conclude that both the Eulerian model and the Monte Carlo model have their own limitations. Due to its grid nature, the Eulerian dispersion model cannot handle the proper parameterization of subgrid scale processes, and therefore produces artificial diffusion

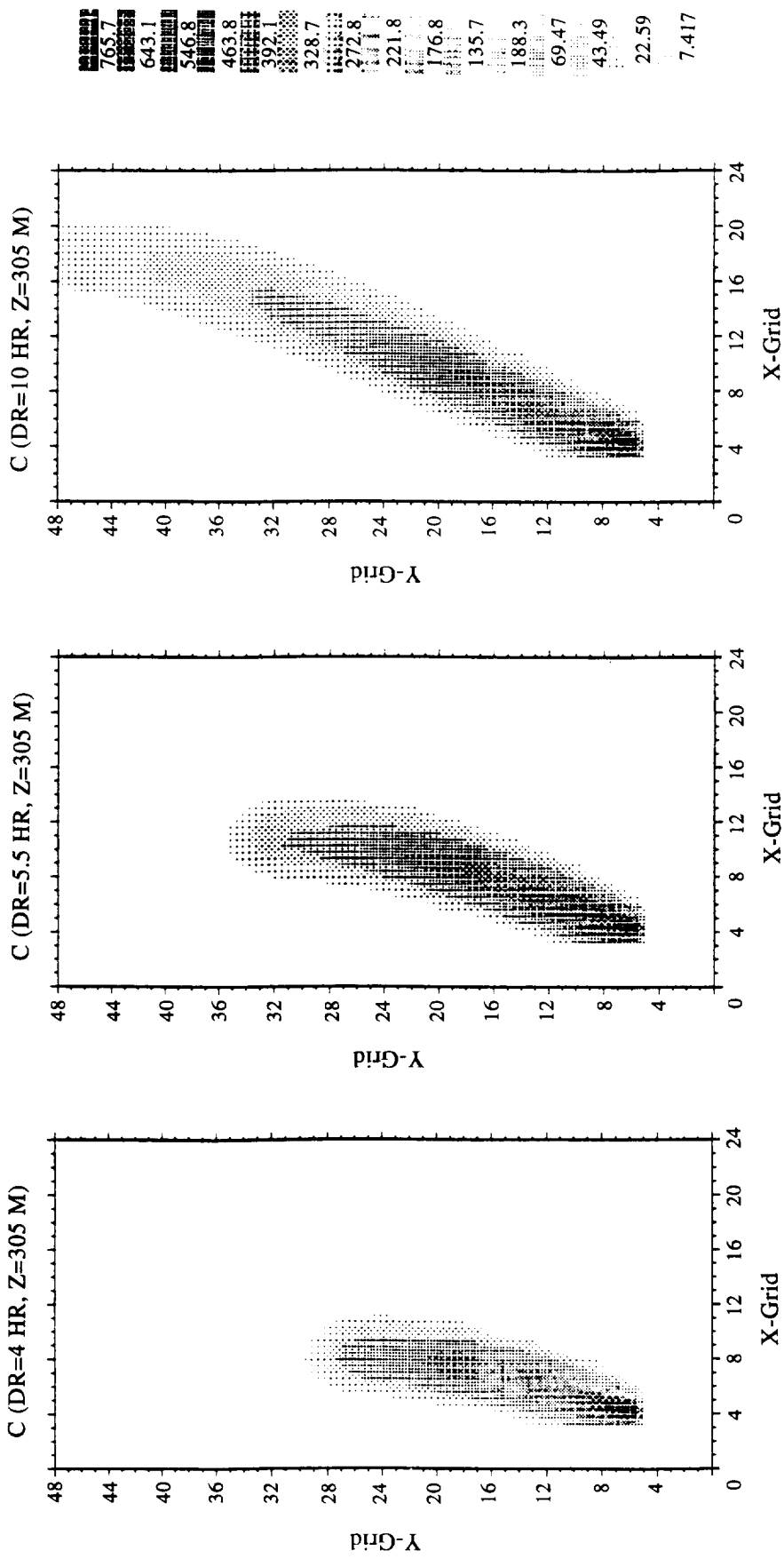

Fig. 10. The Eulerian dispersion model simulated concentration fields after 4, 5.5 and 10 h of the plume travel time for a horizontal plane located at the source height of 305 m.

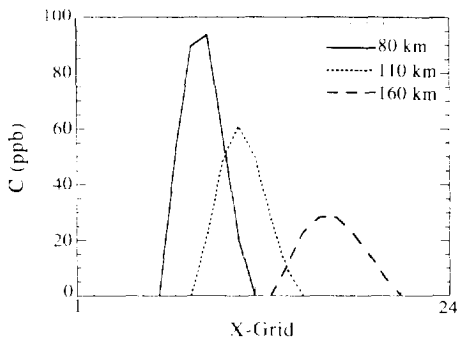

Fig. 11. The Eulerian dispersion model simulated crosswind SO_2 concentrations of the Cumberland plume sampled at 80, 110 and 160 km downwind distances.

(especially near the source). The Monte Carlo dispersion model requires a large number of particles to be released for the long-range transport of pollutants. In order to reduce the limitations of these two dispersion models, both the modeling approaches could be combined to form a hybrid model. The hybrid modeling approach basically uses the Eulerian dispersion model to simulate atmospheric dispersion when the spatial gradients are small, but uses the Monte Carlo dispersion model whenever small-scale features become important. In other words, emissions from a individual point source are treated in a moving Lagrangian framework until they become sufficiently diffuse so that they can be treated accurately in the fixed Eulerian framework.

7. CONCLUSIONS

A modeling system was developed in this study based on coupling a mesoscale meteorological model with a Monte Carlo dispersion model, plus embedding an Eulerian dispersion model into the mesoscale meteorological model. The modeling system was then applied to the Tennessee Plume Study experiments on 23 August 1978.

The results demonstrated that, in general, the modeling system performed satisfactorily. The mesoscale meteorological model reproduced the meteorological fields reasonably well. Both the dispersion models simulated the trajectory of the Cumberland plume well as compared to the observations, while the spread of the plume simulated by the Monte Carlo model was in better agreement with the observations. The results also indicated that the two dispersion modeling approaches (Eulerian and Lagrangian) used in this study have their own limitations. The Eulerian dispersion model simulations indicated that the initial stage of point source emissions cannot be treated properly by the Eulerian model due to its grid nature, while the Monte Carlo model simulations pointed out that the long-range transport of pollutants requires the release of a large number of particles. In order to reduce these limitations, a hybrid model will be developed in the future. The hybrid model will use the Eulerian dispersion model to simulate atmospheric dispersion when the spatial gradients are small, but will use the Monte Carlo model whenever small-scale features become important.

Acknowledgements—The authors wish to thank Dr Noor Gillani of EPA for providing the Tennessee Plume Study data set and for several helpful discussions.

REFERENCES

Bass A. (1980) Modeling long-range transport and diffusion. In *Proc. 2nd Joint Conf. on Applications of Air Pollution Meteorology*, 24–27 March 1980, Boston, Massachusetts, pp. 193–215. American Meteor. Soc. and Air Pollut. Control Assoc.

Bhumralkar C. M. (1975) Numerical experiments on the computation of ground surface temperature in atmospheric general circulation model. *J. atmos. Meteorol.* **14,** 1246–1258.

Boybeyi Z. and Raman S. (1992a) A three-dimensional numerical sensitivity study of convection over the Florida peninsula. *Boundary-Layer Met.* **60,** 325–359.

Boybeyi Z. and Raman S. (1992b) A three-dimensional numerical sensitivity study of mesoscale circulations induced by circular lakes. *Met. Atmos. Phys.* **49,** 19–41

Boybeyi Z., Raman S. and Zannetti P. (1994) A numerical investigation of the possible role of local meteorology in the Bhopal gas accident. *Atmospheric Environment* (in press).

Businger J. A., Wyngaard J. C., Izumi Y. and Bradley E. F. (1971) Flux–profile relationships in the atmospheric surface layer. *J. atmos. Sci.* **28,** 181–189.

Clark R. E., Gillen M. E. and Tibi R. M. (1980) Project STATE–The Tennessee plume study: TVA meteorological analysis. Technical Report, EPA, Washington, DC.

Deardorff J. W. (1978) Efficient prediction of ground surface temperature and moisture with inclusion of a layer of vegetation. *J. geophys. Res.* **83C,** 1889–1903.

Gillani N. V., Kohli S. and Wilson W. E. (1981) Gas-to-particle conversion of sulfur in power plant plumes—I. Parameterization of the conversion rate for dry, moderately ambient conditions. *Atmospheric Environment* **15,** 2293–2313.

Gillani N. V., Pradhan C., El-Ghazzawy O. and Cobourn G. (1979a) Tennessee plume study: data volume of BNL aircraft measurements. Technical Report, STATE Data Center, CAPITA, Washington University, St. Louis, Missouri.

Gillani N. V., Pradhan C., El-Ghazzawy O., Cobourn G., Vaughan W. M., Schillinger D. and Fox R. (1979b) Tennessee plume study: data volume of EMR aircraft measurements. Technical Report, STATE Data Center, CAPITA, Washington University, St. Louis, Missouri.

Hanna S. R. (1982) Applications in modeling. In *Atmospheric Turbulence and Air Pollution Modeling* (edited by Nieuwstadt F. T. M. and van Dop H.), pp. 275–310. D. Reidel, Dordrecht.

Huang C. Y. and Raman S. (1990) Numerical simulations of cold air advection over the Appalachian mountains and the Gulf Stream. *Mon. Weath. Rev.* **118,** 343–362.

Huang C. Y. and Raman S. (1992) A three-dimensional numerical investigation of a Carolina coastal front and the Gulf Stream rainband. *J. atmos. Sci.* **49,** 560–584.

Klemp J. B. and Durran D. R. (1983) An upper boundary condition permeating internal gravity wave radiation in numerical mesoscale model. *Mon Weath. Rev.* **111,** 430–444.

McNider R. T., Moran M. D. and Pielke R. A. (1988) Influence of diurnal and inertial boundary layer oscil-

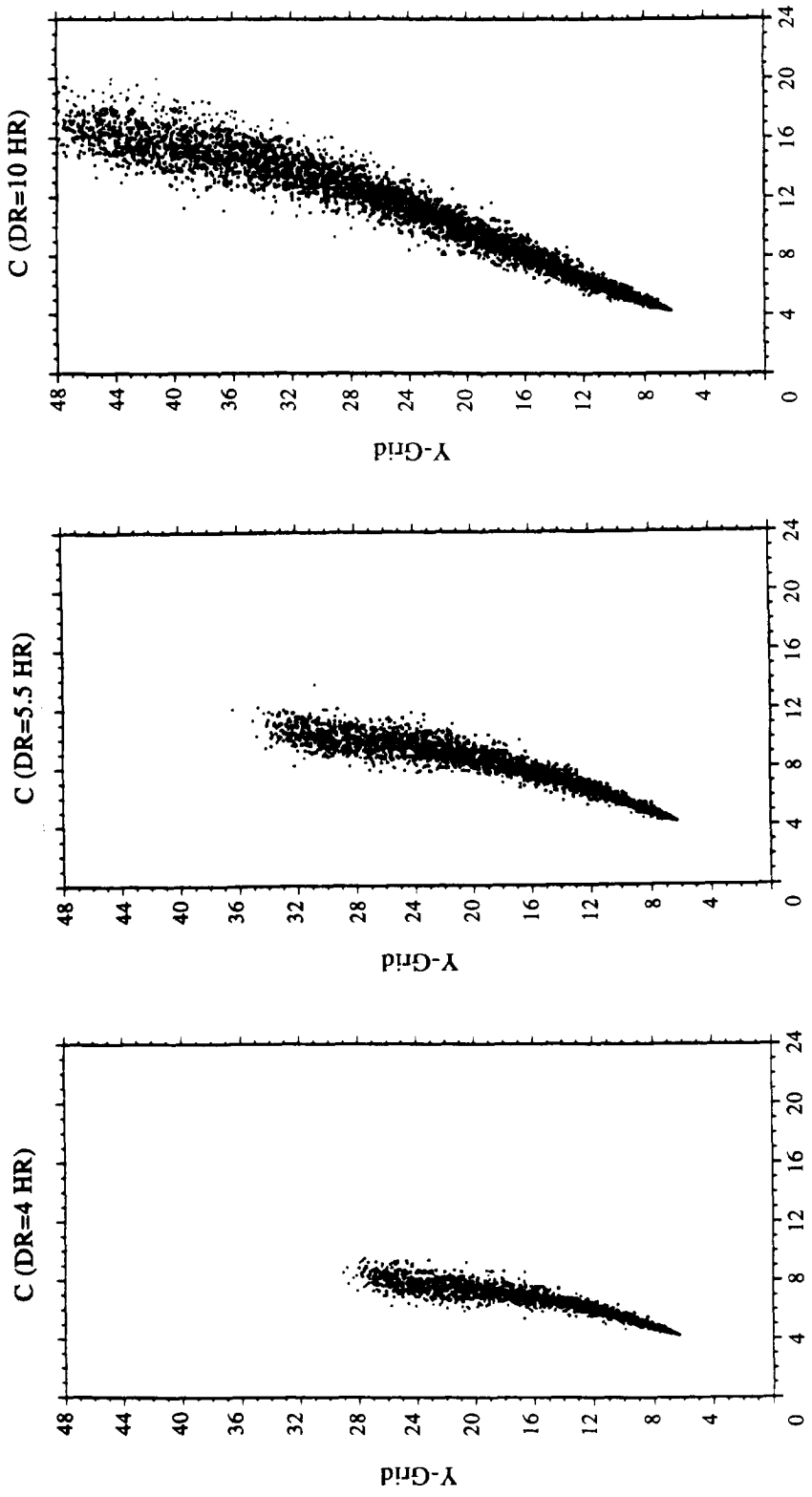

Fig. 12. The Monte Carlo dispersion model simulated particle locations projected on a horizontal plane located at the source height of 305 m after 4, 5.5 and 10 h of the plume travel time.

lations on long-range dispersion. *Atmospheric Environment* **22,** 2445–2462.

Mellor G. L. and Yamada T. (1982) Development of a turbulence closure model for geophysical fluid problems. *Rev. Geophys. Space Phys.* **20,** 851–875.

Miller M. J. and Thorpe A. J. (1981) Radiation conditions for the lateral boundaries of limited area numerical models. *Q. J. R. Met. Soc.* **107,** 615–628.

Orlanski I. (1976) A simple boundary condition for unbounded hyperbolic flows. *J. Comput. Phys.* **21,** 251–269.

Pack D. H., Ferber G. J., Heffter J. L., Telegadas K., Angell J. K., Hoecker W. H. and Machta L. (1978) Meteorology of long range transport. *Atmospheric Environment* **12,** 425–444.

Pielke R. A. (1984) *Mesoscale Meteorological Modeling,* 612 pp. Academic Press, New York.

Warming R. F., Kutler P. and Lomax H. (1973) Second- and third-order noncentered difference schemes for nonlinear hyperbolic equations. *AIAA J.* **11,** 189–196.

Zannetti P. (1984) A new Monte-Carlo scheme for simulating Lagrangian particle diffusion with wind shear effects. *App. Math. Modelling* **8,** 188–192.

Zannetti P. (1986) Monte-Carlo simulation of auto- and cross-correlated turbulent velocity fluctuations (MC-LAGPAR II Model). *Environ. Software* **1,** 26–30.

Zannetti P. (1990) *Air Pollution Modelling,* 444 pp. Van Nostrand Reinhold, New York.